Journal of Power Sources 196 (2011) 10673–10678

Contents lists available at SciVerse ScienceDirect

Journal of Power Sources

journal homepage: www.elsevier.com/locate/jpowsour

Nickel foam supported Sn–Co alloy film as anode for lithium ion batteries

Chenge Yang[a], Dawei Zhang[a,*], Yongbin Zhao[a], Yuhao Lu[b], Long Wang[b], John. B. Goodenough[b,**]

[a] School of Chemical Engineering, Hefei University of Technology, Hefei 230009, PR China
[b] Texas Materials Institute, The University of Texas at Austin, 1 University Station, C2201, Austin, TX 78712, United States

ARTICLE INFO

Article history:
Received 8 April 2011
Received in revised form 1 July 2011
Accepted 22 August 2011
Available online 27 August 2011

Keywords:
Electrochemical deposition
Lithium ion battery
Nickel foam
Capacity retention
Heat treatment

ABSTRACT

Sn–Co alloy films are deposited electrochemically directly onto nickel foam in an aqueous solution. The influence of electrochemical current density and heat treatment on the structure and morphology of the electrodeposited films is studied by X-ray diffraction (XRD) and scanning electron microscopy (SEM). The electrochemical properties of the Sn–Co alloy films are further investigated by galvanostatic charge–discharge tests. As anodes for lithium ion batteries, the Sn–Co alloy-film anodes, after further heat treatment at 200 °C for 30 min, delivers a specific capacity of 663 mAh g^{-1} after 60 cycles. This high capacity retention is attributed to the unique electrode configuration with an enhanced interface strength between the active material and the current collector formed in the heat-treatment process.

1. Introduction

Recently, tin-based alloys have drawn considerable attention as promising alternative anodes for lithium ion batteries (LIBs) because of their higher specific capacity than traditional graphite materials and their better cycling ability than pure tin anodes [1,2]. However, the irreversible capacity in the first charge process and the volume expansion followed by a conductivity degradation during charge and discharge cycling are still obstacles to commercialization [3]. Two strategies have been adopted to overcome the electrode deterioration caused by the volume expansion, designing nanostructured electrode materials [4–11] and use of intermetallic tin-based compounds [12–29]. The reaction of intermetallic Sn_xM_Y with lithium involves formation of brittle Li–Sn alloys. The relatively inactive metal, M, plays the role of matrix buffer, which effectively suppresses the large volume expansion during the alloying/dealloying process. Accordingly, the intermetallic tin-based materials exhibit a much greater electrochemical capacity than that of a pure tin or graphite electrode.

Various methods have been used to fabricate tin-based alloy materials, such as high-energy ball milling [6,9–11], chemical reduction [4,12] and solid-state reaction [15,16]. Obtaining the intermetallic tin-based alloys by electrochemical deposition is relatively simple and inexpensive; it can also provide a stable electrochemical capacity [17–28]. Hassoun et al. [18] synthesized Sn–Ni film electrodes on Cu foil that showed a capacity of 550 mAh g^{-1} after 40 cycles. Tamura et al. [23,24] fabricated an amorphous Sn–Co alloy film by electrocodeposition on Cu foil with a rough surface; the specific capacity of their electrode retained 600 mAh g^{-1} after 20 cycles.

In this work, Sn–Co alloy films were electrochemically deposited on nickel foam in aqueous solution. Used as current collectors, the nickel foam with a three-dimensional network structure not only increases the electrical conductivity. It also avoids the macrostructural deformation for the tin based electrodes and buffers the large volume change during lithium insertion and extraction [30]. We report the influence on the electrochemical properties of morphological changes of the Sn–Co alloy films on the nickel foam obtained with different current density and heat treatment.

2. Experimental

2.1. Electrochemical fabrication of Sn–Co film on nickel foam

Nickel foam was used as the metal substrate. As shown in Fig. 1A and B, foamed nickel has a three-dimensional grid structure and shows a high porosity and specific surface area with considerable and uniform strength.

The Sn–Co alloy samples were deposited electrochemically on the nickel foam in a two-electrode cell at 50 °C; a graphite plate was used as the counter electrode. The electrodeposition solution consisted of $SnCl_2{\cdot}2H_2O$ (25 g L^{-1}), $CoCl_2{\cdot}6H_2O$ (25 g L^{-1}), $K_4P_2O_7{\cdot}3H_2O$ (300 g L^{-1}) and an additive agent (10 g L^{-1}). All these reagents are analytical. The electrodeposition current density was

* Corresponding author. Tel.: +86 551 2901450; fax: +86 551 2901450.
** Corresponding author. Tel.: +1 512 471 1646; fax: +1 512 471 1646.
E-mail addresses: zhangdw@ustc.edu.cn (D. Zhang), jgoodenough@mail.utexas.edu (John.B. Goodenough).

0378-7753/$ – see front matter © 2011 Elsevier B.V. All rights reserved.
doi:10.1016/j.jpowsour.2011.08.089

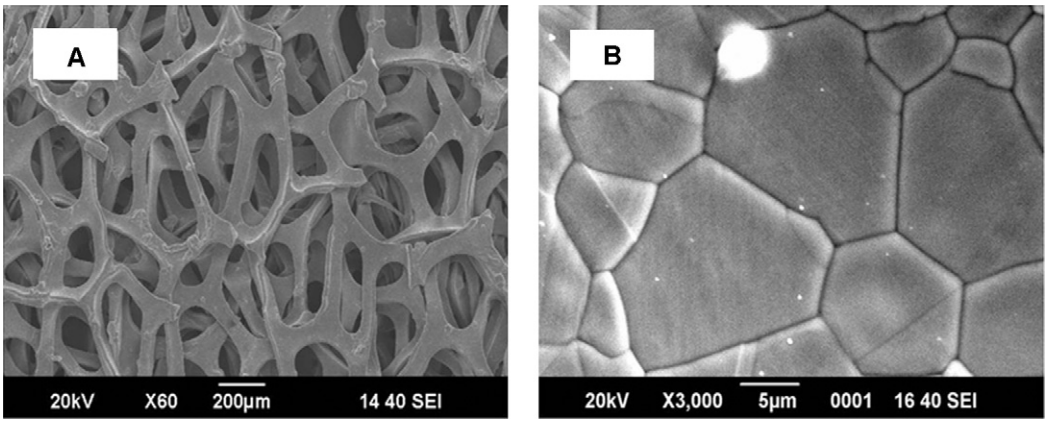

Fig. 1. (A) SEM images of the nickel foam. (B) Nickel foam surface.

monitored by a potentiostat/galvanostat (HDV-7C). The Sn–Co alloy samples were annealed at 200°C for 30 min in a nitrogen atmosphere. The weight of the active material in the investigated anodes was measured by analyzing the amount of tin contained in them by ICP spectrometry.

2.2. Electrochemical performance

The electrochemical performance of the Sn–Co films was investigated in two-electrode coin cells (CR2032) of Li|1 M $LiPF_6$ (EC:DEC = 1:1)|Sn–Co alloy; a Celgard 2400 microporous polypropylene membrane was used as separator. These CR2032 cells were assembled in an argon-filled glove box. These cells were cycled galvanostatically at room temperature between 0 and 1 V on a multi-channel battery test system (NEWARE BTS-610) with a current density of 0.4 mA cm^{-2}.

2.3. Morphological and structural characterization of the Sn–Co films

The as-prepared samples were characterized by scanning electron microscopy (SEM, Hitch X650), and X-ray diffraction (XRD, Philips X'Pert Pro Super X-ray diffractometer, Cu-Kα radiation). X-ray fluorescence spectroscopy (XRF, XRF-1800) was also carried out to certify the surface composition. To investigate with SEM the morphology change after charge–discharge cycling, the cycled electrodes were washed with diethyl carbonate (DEC) to remove the residual electrolyte and transferred to the SEM.

3. Results and discussion

3.1. Morphological and structural characterization of the Sn–Co films

In order to investigate the influence of the electrodeposition parameters on the morphology and structure of the Sn–Co alloy films supported on nickel foam, three Sn–Co alloy samples were synthesized under the current density of 10 mA cm^{-2}, 30 mA cm^{-2} and 50 mA cm^{-2} and named as SnCo-1, SnCo-2 and SnCo-3, respectively. To obtain Sn–Co films with similar film thickness we varied the electrodeposition time for different current densities. The electrodeposition time was 5 min, 8 min and 10 min, respectively. The obtained Sn–Co films have similar film thickness of 6 μm. In addition, to investigate the influence of heat treatment, the three samples were then annealed at 200 °C for 30 min, named as SnCo-4, SnCo-5 and SnCo-6, respectively.

Fig. 2 shows the XRD patterns of the six Sn–Co alloy samples. Without heat-treatment, there are no obvious diffraction peaks of the Sn–Co phase for SnCo-1, -2, -3. This should be due to the weak crystallinity of the active materials. However, after heat treatment at 200 °C for 30 min in nitrogen atmosphere, a small peak appeared, which is reported to be from the amorphous Sn and Co phase [22]. The active material is considered to be an amorphous Sn–Co alloy where both Sn and Co atoms are dispersed uniformly [22]. From an analysis of X-ray fluorescence spectroscopy, the Sn–Co alloy was composed of 75% Sn and 25% Co in mass%, indicating that an intermetallic compound of Co_2Sn_3 has been obtained under present conditions.

Fig. 3 shows the top-view morphologies of the six Sn–Co alloy samples. It can be seen that without heat treatment a different morphology of the Sn–Co alloy samples is obtained under different current density and time conditions. Sample SnCo-1 obtained at current density of 10 mA cm^{-2} for 10 min presented a highly rough surface with agglomerated particles on the substrate (Fig. 3A), and a porous noncrystalline phase can be observed for sample SnCo-2 at current density of 30 mA cm^{-2} for 3 min (Fig. 3B). On increasing the current density to 50 mA cm^{-2}, the sample SnCo-3 formed compactly with aggregates of small spherules rather than rough-surfaced particles, as is shown in Fig. 3C. However, after the heat treatment at 200 °C for 30 min in nitrogen atmosphere, all the samples formed continuous alloy films due to re-reaction under the melting condition at 200 °C.

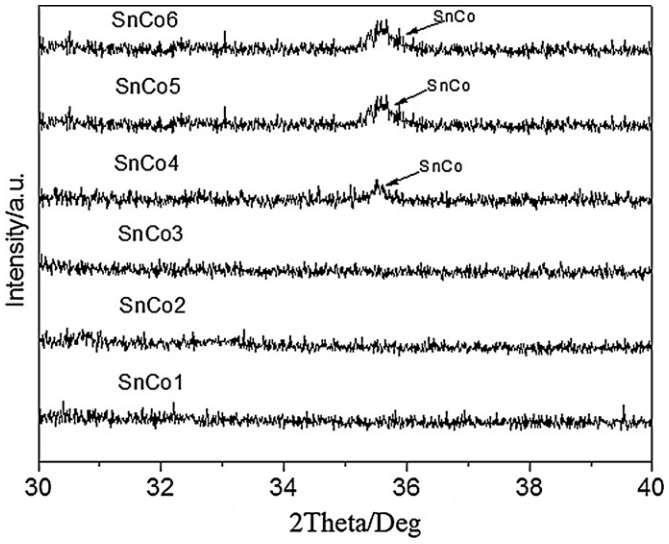

Fig. 2. The XRD patterns of the six Sn–Co alloy samples. SnCo-1; SnCo-2; SnCo-3; SnCo-4; SnCo-5 and SnCo-6.

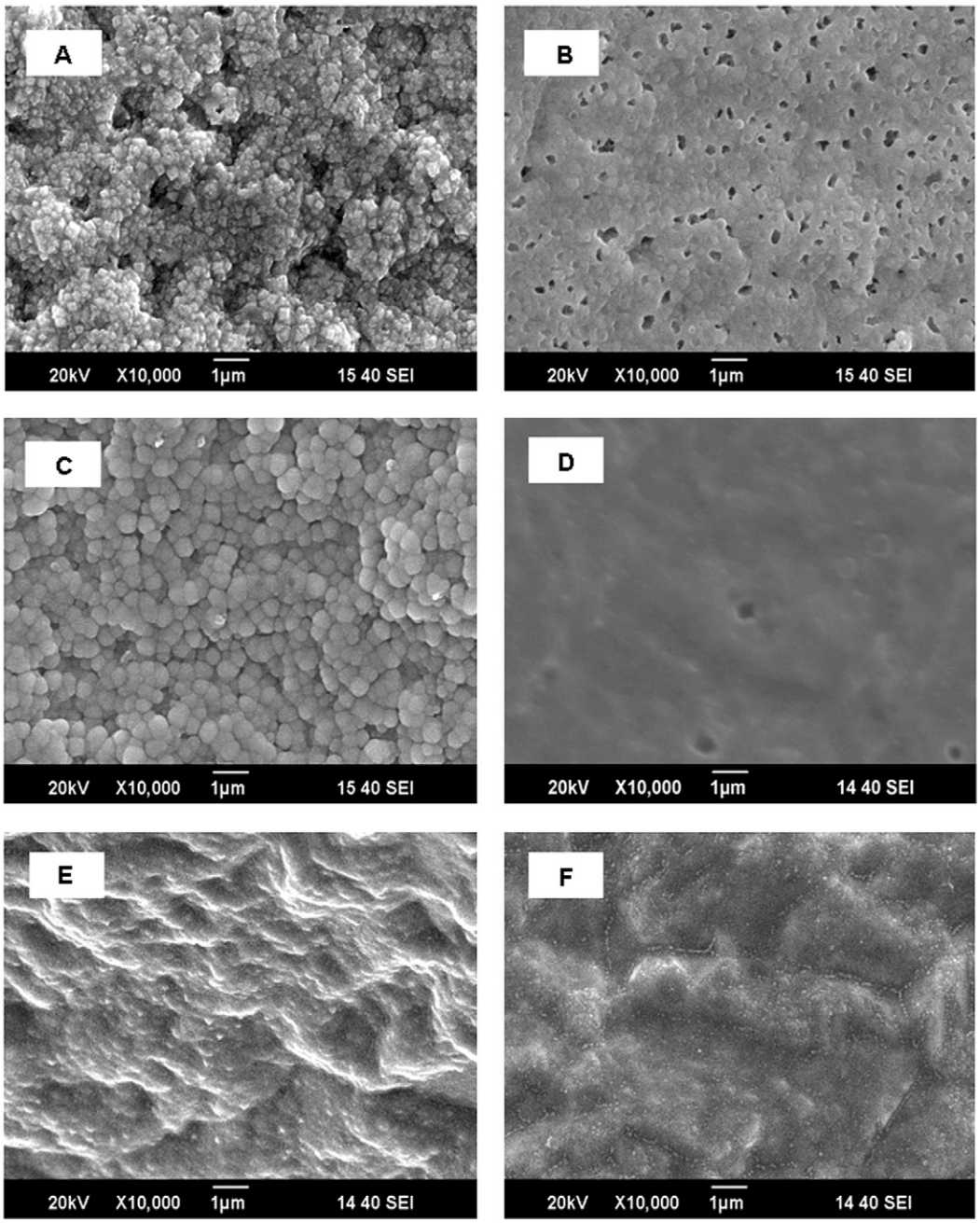

Fig. 3. SEM images of top views of the six Sn–Co alloy samples. SnCo-1 (A); SnCo-2 (B); SnCo-3 (C); SnCo-4 (D); SnCo-5 (E) and SnCo-6 (F).

3.2. Electrochemical performance of the Sn–Co alloy films in lithium batteries

Fig. 4 shows the cyclic voltammograms (CVs) of the six Sn–Co alloy film electrodes at a scanning rate of 0.2 mV s^{-1}. In the first discharge step (Fig. 4A), all the curves show a process occurring at 1.0–1.25 V corresponding to the formation of the solid electrolyte interface (SEI) layer on the surface of the electrode. The organic electrolyte containing EC could be reduced to form lithium carbonate and lithium alkyl carbonate at this low potential. The large reduction peak from 0.25 V to 0 V should be attributed to the reversible reaction of Sn–Co with metallic lithium into $Li_{4.4}Sn$ and metallic cobalt [31–33]. It's not regular that there is only one reduction peak in the first discharge process. Since it's not a steady discharge process for the first cycle; the active materials on the nickel foam will be soaked by the electrolyte and be activated for some time. So, the discharge potential of the first cycle shifted to negative and its profile showed a different shape in the first cycle [21,33,34]. An obvious oxidation peak was observed on the cathodic run; it corresponds to the lithium extraction reaction from the alloy formed in the first discharge cycle. In addition, during the second and third charge/discharge cycles, the small peak at 1.2 V in the first discharge process disappears, indicating that a stable SEI layer had been formed on the electrode; the irreversible capacity disappeared completely. The currents of annealed electrodes (SnCo-4, -5, -6) are smaller than those of as-prepared electrodes (SnCo-1, -2, -3). The origin is the difference in the crystallinity of Sn–Co caused by the heat treatment.

Fig. 5 shows the voltage versus specific capacity profiles of the Sn–Co alloy/Li cells at 0.2 C cycling rate during the first discharge/charge cycle. In the first discharge step, all the curves show a process occurring at 1.0–1.30 V corresponding to the formation

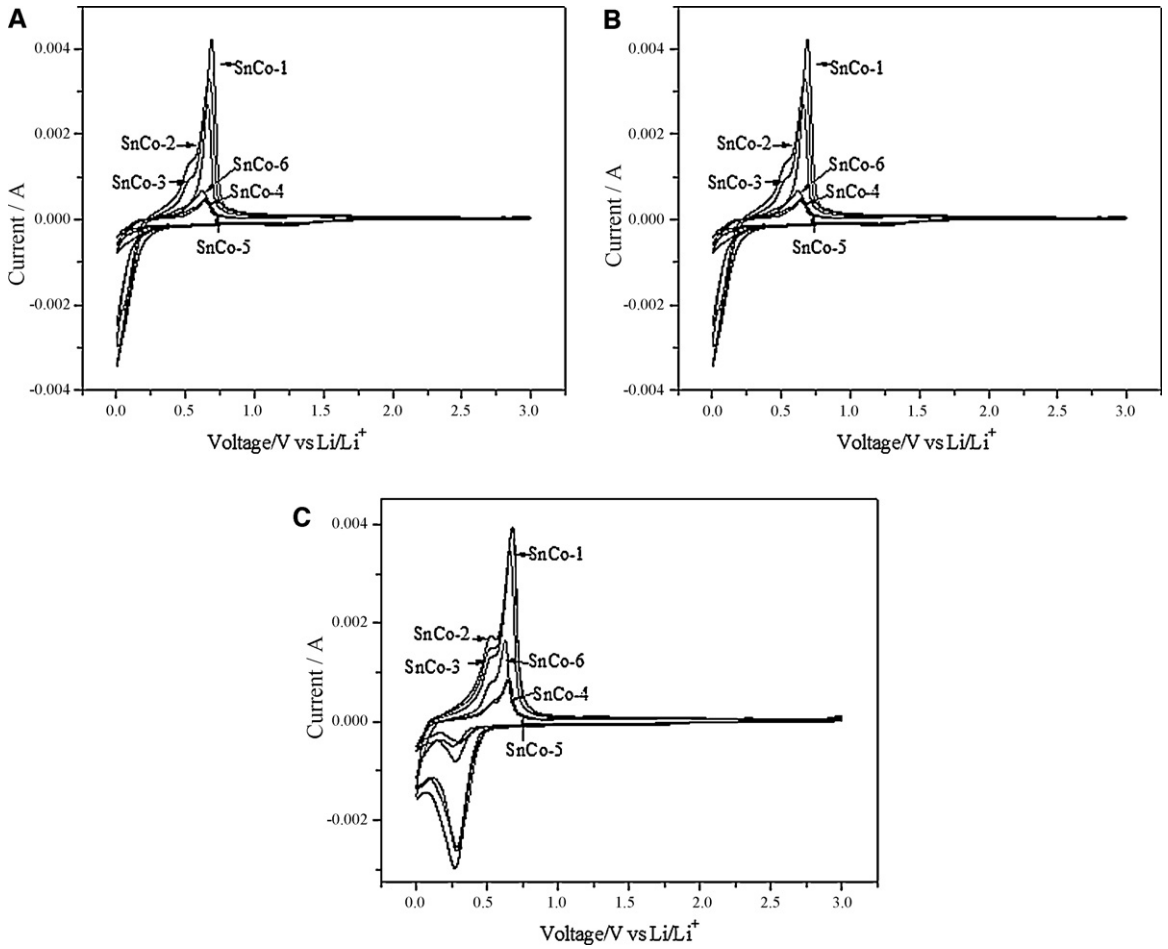

Fig. 4. Cyclic voltammograms of the six Sn–Co alloy samples. The scanning rate is 0.2 mV s^{-1}. The voltage ranges from 3 V to 0 V. The first cycle (A); the second cycle (B); the third cycle (C).

of the solid electrolyte interface (SEI) layer on the surface of the electrode [27,29,31]. The specific capacity of all six Sn–Co alloy samples during the first discharge process is higher than the theoretical value of 744 mAh g^{-1} according to a consumption of 13.2 lithium ions per Co_2Sn_3 formula, which can be ascribed to the formation of the SEI layer and the reversible formation of polymeric gel-like films [35,36]. After the first charge process, the coulombic efficiencies for the non-heated samples (SnCo-1, SnCo-2 and SnCo-3) are, respectively, 76.1%, 66.3% and 75.5%. This high irreversible capacity corresponds to the large electrode surface for formation of the SEI layer, which consumes lithium ions. For the heated samples (SnCo-4, SnCo-5 and SnCo-6), the coulombic efficiency of the first cycle is 54.2%, 66.5% and 53.7%, much less than the non-heated samples, which indicates that the percentage of the irreversible loss to the

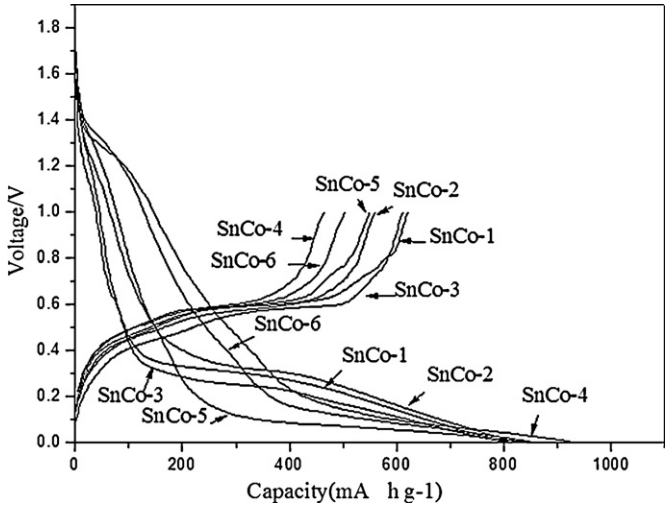

Fig. 5. Voltage versus capacity profiles of the six Sn–Co samples for the first discharge–charge cycle (OCV-0 V at current of 0.4 mA cm^{-2}).

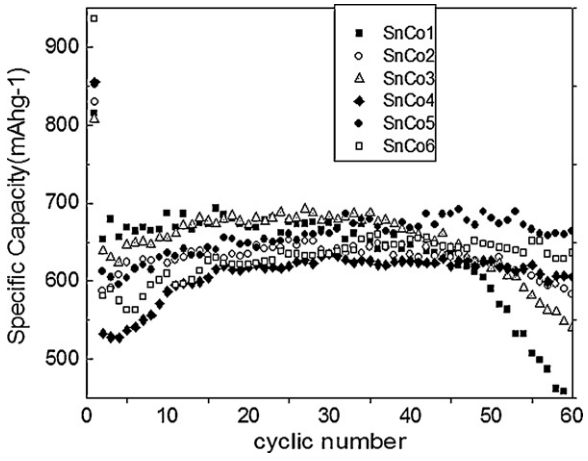

Fig. 6. Specific capacity of cycle number for the six Sn–Co/Li cells.

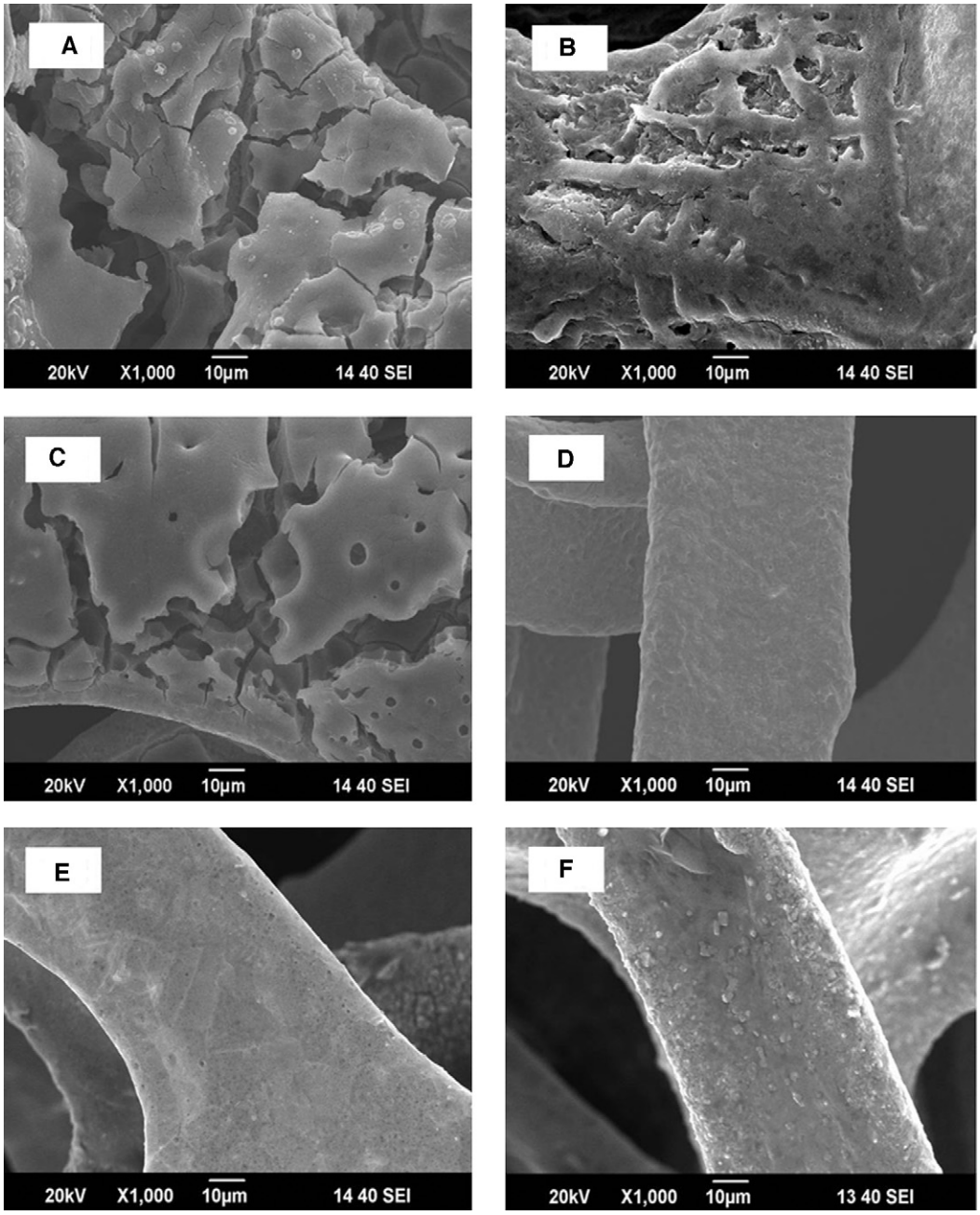

Fig. 7. SEM images of the Sn–Co alloy samples after 40 cycles. SnCo-1 (A); SnCo-2 (B); SnCo-3 (C); SnCo-4 (D) SnCo-5 (E); SnCo-6 (F).

SEI layer is greater for a thin continuous alloy film than for an alloy of small particles.

The electrochemical performances of the six Sn–Co alloy samples are shown in Fig. 6. We can observe an increase in capacity in the first several cycles. The interesting phenomenon of an initial capacity drop followed by a gradual increase is well-known [37]; it results from some irreversible Li_2O generated in the first discharge step [35]. All the samples delivered a steady capacity from the second cycle until 50th cycle, more than 620 mAh g^{-1}. This reversible capacity is higher than that reported in the literature, which shows the superiority of fabricating this anode by electrodeposition directly on foam nickel. Firstly, this higher reversible capacity benefits from improved electronic conductivity between the active material and the current collector compared to an anode fabricated by the conventional slurry coating process. Secondly, the macroporous Sn–Co alloy electrode may provide a barrier against the aggregation of Sn into large grains during Li-ion insertion and extraction processes. It is obvious that the porous structure can also accommodate the volume expansion due to the phase transition during Li insertion, which improves significantly the cycling life of the electrode and is beneficial to diffusion of Li-ions in insertion/extraction processes.

However, from the 50th cycle the discharge capacity for the three non-heated samples (SnCo-1, SnCo-2 and SnCo-3) began to decrease remarkably. In the 60th cycle their discharge capacity retention was, respectively, 54.4%, 70.3% and 65.8%, in which only SnCo-2 sustained a high capacity. But the three annealed electrodes (SnCo-4, SnCo-5 and SnCo-6) still had a steady capacity retention of 70.8%, 77.8% and 67.9% even after 60 cycles. This result indicates that the heat treatment process can improve the cycle performance of this alloy anode. It is assumed that this improvement is because the interface strength between the entire part of the active material

and the current collector is enhanced by the heat treatment so that the annealed electrodes can still be active after 60 cycles.

The improved cycling performance for the three samples SnCo-4, SnCo-5 and SnCo-6 can also be seen from the changes of the corresponding morphology. Fig. 7 shows the SEM images of the Sn–Co alloy samples after 50 cycles. Comparison of Fig. 3A and C with Fig. 7A and C shows that films without heat treatment formed "island" structures that broke off from the foam substrate after 40 cycles. The porous structure of the sample SnCo-2 (Fig. 3B) provided a larger surface to volume ratio for accommodation of the volume change and blocking of Sn agglomeration. Therefore, the sample SnCo-2 took on a better buffer function to prevent the film electrodes from pulverizing after 50 cycles. On the other hand, after being heat treated in nitrogen atmosphere, the interface bonding between the entire part of the active material and the current collector is enhanced and continuous SnCo alloy films are formed. After 60 cycles, the active material remains tightly bound to the foam nickel, resulting in a stable discharge capacity of above 600 mAh g^{-1} after 60 cycles.

4. Conclusions

A series of Sn–Co alloy films supported on nickel foam as anode for Lithium ion batteries were deposited electrochemically on nickel foam in an aqueous solution. The morphology of the electrodeposited films was affected by the electrochemical deposition current density and time. Nevertheless, all formed continuous films after heat-treatment at 200 °C for 30 min in nitrogen atmosphere. The capacity and cycling performances of these macroporous Sn–Co alloy films were significantly enhanced. The results also showed that heat treatment could furtherly improve the electrochemical properties. By galvanostatic cell cycling, the Sn–Co alloy film anodes, after further heat treatment, showed a specific capacity of 663 mAh g^{-1} after 60 cycles. This high capacity retention is attributed to the particular structure with considerable strength and tenacity of the three-dimensional nickel foam and the smooth, compact surface formed in the heat treatment process.

Acknowledgements

Financial support from National Science Foundation of China (grant no. 20703013) and the Robert A. Welch Foundation (grant #F-1066), are gratefully acknowledged. D.Z. also thanks the Postdoctor Science Foundation of China (grant no. 20070410219) and the support from China Scholarship Council.

References

[1] I.A. Courtney, J.R. Dahn, J. Electrochem. Soc. 144 (1997) 2045–2052.
[2] Y. Idota, T. Kubota, A. Matsufuji, Y. Maekawa, T. Miyasaka, Science 276 (1997) 1395–1397.
[3] I.A. Courtney, J.R. Dahn, J. Electrochem. Soc. 144 (1997) 2943–2948.
[4] D.G. Kim, H. Kim, H.J. Sohn, T. Kang, J. Power Sources 104 (2002) 221–225.
[5] H. Li, L.H. Shi, W. Lu, X.J. Huang, L.Q. Chen, J. Electrochem. Soc. 148 (2001) A915–A922.
[6] Y. Zheng, J. Yang, Y.N. NuLi, J.L. Wang, J. Power Sources 174 (2007) 624–627.
[7] J. Hassoun, G. Derrien, S. Panero, B. Scrosati, Adv. Mater. 20 (2008) 3169–3175.
[8] H.J. Kim, J. Cho, J. Electrochem. Soc. 154 (2007) A462–A466.
[9] P.P. Ferguson, A.D.W. Todd, J.R. Dahn, Electrochem. Commun. 10 (2008) 25–31.
[10] J. Hassoun, P. Ochal, S. Panero, G. Mulas, C. Bonatto Minell, B. Scrosati, J. Power Sources 180 (2008) 568–575.
[11] J. Hassoun, G. Mulas, S. Panero, B. Scrosati, Electrochem. Commun. 9 (2007) 2075–2081.
[12] F. Wang, M.S. Zhao, X.P. Song, J. Power Sources 175 (2008) 558–563.
[13] A.D.W. Todd, R.E. Mar, J.R. Dahn, J. Electrochem. Soc. 154 (2007) A597–A604.
[14] D.T. Shieh, J.T. Yin, K. Yamamoto, M. Wada, S. Tanase, T. Sakaia, J. Electrochem. Soc. 153 (2006) A106–A112.
[15] L. Simonin, U. Lafont, E.M. Kelder, J. Power Sources 180 (2008) 859–863.
[16] H. Guo, H.L. Zhao, X.D. Jia, J.C. He, W.H. Qiu, X. Li, J. Power Sources 174 (2007) 921–926.
[17] H.P. Zhao, C.Y. Jiang, X.M. He, J.G. Ren, C.R. Wan, Electrochim. Acta 52 (2007) 7820–7826.
[18] J. Hassoun, S. Panero, B. Scrosati, J. Power Sources 160 (2006) 1336–1341.
[19] C. Arbizzani, M. Lazzari, M. Mastragostino, J. Electrochem. Soc. 152 (2005) A289–A294.
[20] H.C. Shin, M.L. Liu, Adv. Funct. Mater. 15 (2005) 582–586.
[21] L.B. Wang, S. Kitamura, T. Sonoda, K. Obata, S. Tanase, T. Sakaia, J. Electrochem. Soc. 150 (2003) A1346–A1350.
[22] N. Tamura, M. Fujimoto, M. Kamino, S. Fujitani, Electrochim. Acta 49 (2004) 1949–1956.
[23] N. Tamura, Y. Kato, A. Mikami, M. Kamino, S. Matsuta, S. Fujitani, J. Electrochem. Soc. 153 (2006) A2227–A2231.
[24] N. Tamura, Y. Kato, A. Mikami, M. Kamino, S. Matsuta, S. Fujitani, J. Electrochem. Soc. 153 (2006) A1626–A1632.
[25] F.S. Ke, L. Huang, H.H. Jiang, H.B. Wei, F.Z. Yang, S.G. Sun, Electrochem. Commun. 9 (2007) 228–232.
[26] F.S. Ke, L. Huang, J.S. Cai, S.G. Sun, Electrochim. Acta 52 (2007) 6741–6747.
[27] F.S. Ke, L. Huang, H.B. Wei, J.S. Cai, X.Y. Fan, F.Z. Yang, S.G. Sun, J. Power Sources 170 (2007) 450–455.
[28] D.W. Zhang, C.G. Yang, J. Dai, J.W. Wen, L. Wang, C.H. Chen, Trans. Nonferrous. Met. Soc. China 19 (2009) 1489–1493.
[29] M. Wachtler, M. Winter, J.O. Besenhard, J. Power Sources 105 (2002) 151.
[30] M. Yoshio, T. Tsumura, N. Dimov, J. Power Sources 146 (2005) 10.
[31] M. Winter, J.O. Besenhard, Electrochim. Acta 45 (1999) 31.
[32] R.A. Huggins, J. Power Sources 81–82 (13.) (1999).
[33] N. Tamura, R. Ohshita, M. Fujimoto, M. Kamino, S. Fujitani, J. Electrochem. Soc. 150 (2003) A679.
[34] N. Tamura, R. Ohshita, M. Fujimoto, S. Fujitani, M. Kamino, I. Yonezu, J. Power Sources 107 (2002) 48.
[35] Y. Yu, C.H. Chen, J.L. Shui, S. Xie, Angew. Chem. Int. Ed. 44 (2005) 7085.
[36] H.C. Liu, S.K. Yen, J. Power Sources 166 (2007) 478.
[37] W.Y. Li, L.N. Xu, J. Chen, Adv. Funct. Mater. 15 (2005) 851.